J Mater Sci (2011) 46:7905–7911
DOI 10.1007/s10853-011-5907-8

LETTER

In situ synthesis of high-density contact-free Ag-nanoparticles for plasmon resonance polystyrene nanocomposites

Daniele Pullini · Gianfranco Carotenuto · Mariano Palomba · Alessandra Mosca · Andy Horsewell · Luigi Nicolais

Received: 5 July 2011 / Accepted: 25 August 2011 / Published online: 9 September 2011

In the last decades, polymer matrix nanocomposites (PMN) have been studied extensively to exploit the properties of nanofillers for transforming the nature of practical household materials, in particular for mechanical properties [1]. Despite the early successes [2], the massive interest in nanocomposites started in 1990s, when Toyota proved that adding mica to nylon produced a fivefold increase in the yield and tensile strength of the matrix material [3, 4]. Subsequent developments further contributed to the surging interest in polymer–nanoparticle composites. In particular, the growing availability of nanoparticles of monodispersed size and shape, such as fullerenes, carbon nanotubes, inorganic nanoparticles, dendrimers, and bio-nanoparticles, and the refining of instrumentation to probe nano-objects, such as scanning force, laser scanning fluorescence, and electron microscopes, have spurred research aimed at probing the influence of particle size and shape on the properties of PMN also for functional applications: optics, photonics, catalysis, electronic devices, and Microsystems [5, 6]. A sub-class of PMN is represented by the metal–polymer nanocomposites (hereinafter MPN) which directly harness the fundamental properties of metal nanoparticles when embedded in a polymer matrix. There is a widespread interest in this material class especially for the optical and photonic fields uses including: eye and sensor protection [7], optical communications [8], optical information processing [9], Raman enhancement materials [10], optical switching [11, 12], plasmon waveguides [13, 14], light stable colour filters [15, 16], polarisers [17], and modified refractive index materials [18]. Particularly, for all the applications mentioned above, the spectroscopy properties of silver nanoparticles are extremely useful; therefore, Ag-nanoparticles have been extensively modelled [19] and characterized when suspended in liquid media [20, 21]. Depending on the particle diameters and the surrounding medium the Ag-based colloids exhibit narrow and intense surface plasmon resonance (SPR) displaying selective absorption of visible radiation which are found suitable to develop a novel class of optical limiters and filters. In fact, it is generally acknowledged that the optical excitation of plasmon resonances in nanosized Ag particles is the most efficient mechanism by which light interacts with matter—a single Ag nanoparticle interacts with light more efficiently than a particle of the same size of any known chromophore. Silver is also the only material whose plasmon resonance can be tailored to any wavelength in the visible spectrum [22]. For all these reasons, in this study, silver was chosen as a nanofiller to develop a novel class of SPR material to be employed in a number of automotive components such as optical filtering glasses and micro-optical-electro-mechanical systems (MOEMS).

The most common approach to have PMN synthesized is based on the dispersion of pre-synthesized nanoparticles into a polymer matrix, namely: ex-situ nanoparticle synthesis followed by mixing into the matrix. The greatest

D. Pullini · M. Palomba
Group Materials Labs, Fiat Research Centre Scpa, Strada Torino 50, 10043 Orbassano, Italy

G. Carotenuto (✉) · M. Palomba · L. Nicolais
Institute of Composite and Biomedical Materials, National Research Council, Piazzale Tecchio, 80, 80125 Naples, Italy
e-mail: giancaro@unina.it

A. Mosca · A. Horsewell
Department of Mechanical Engineering & Center for Electron Nanoscopy, Technical University of Denmark, 2800 Kongens Lyngby, Denmark

L. Nicolais
Department of Materials and Production Engineering, University of Naples 'Federico II', P.le Tecchio 80, 80125 Naples, Italy

stumbling block to the large-scale production and commercialization of these materials is the dearth of cost-effective methods for controlling the dispersion of the nanoparticles in the polymeric hosts. The nanoscale particles typically aggregate, which then removes any benefits associated with the nanoscopic dimension. There is a critical need for establishing processing techniques that are effective on the nanoscale yet are applicable to macroscopic processing. The interactions of nanoparticles with polymers are mediated by ligands attached to the nanoparticles; thus, the ligands markedly influence particle behaviour and spatial distribution. The surface chemistry of nanoparticle functionalization representing, in all cases, an additional production cost could only partly solve the aforementioned problems and today only a very small concentration (about 0.1 wt%) of nanofillers can be fully dispersed within a polymer matrix without aggregating. As for all PMN types, at the beginning, metal–polymer and ceramic–polymer nanocomposites were developed by an ex-situ approach [23]. By these methods, to prevent the nanoparticles from oxidation, colloidal chemistry techniques were used to synthesize aqueous nanoparticle suspensions, which required surface modification by silanization or similar treatments (thiol absorption, etc.), followed by drying and re-dispersion in a molten thermoplastic polymer or a liquid monomer to be successively polymerized. This approach had the disadvantage of leaving aggregated nanoparticle systems which resulted in being inadequate for practical applications. An effective alternative to the ex-situ approach is the in situ preparation of PMN consisting of the formation of separate nanoparticles inside a polymer matrix. This approach presents three main advantages compared to the ex-situ one: (i) particle nucleation takes place in a molten polymeric phase and therefore at very high temperatures (200–300 °C), consequently extremely small clusters are generated owing to the involved high nucleation rate; (ii) the nanoparticle diffusivity is low in a viscous molten polymer and consequently Brownian motion is limited and nanoparticle aggregation is negligible; (iii) usually, thermoplastic polymer processing is based on the material being heated and the in situ preparation of metal nanoparticles is based on thermal decomposition of organic salts or organometallic complexes and therefore a scaling up of the process can be easily done. The first class of thermolytic precursors for the in situ generation of metal nanoparticles was based on metal carbonyl species (i.e., $Me_x(CO)_y$); subsequently, mercaptides (that is, salts of thiols, $Me(SR)_x$) were used as precursors for noble-metals and semimetal nanoparticles [23] as they are soluble in non-polar polymer matrices and decompose at temperatures compatible with polymer thermal stability (100–200 °C). Other organometallic species have been occasionally used like cupferronates, acetilides, etc. [23]. For the specific case of Ag–PN the potentials of the technique have not been harnessed in depth, the precursors investigated include silver alkanoates [24, 25], silver acetate [26, 27], silver perfluorocarboxylates [28], silver oxalate [29], Ag(hfa)tetraglyme [30], silver nitrate [31], and silver carboxylates [32–35]. The reported methods often require high temperatures (120–250 °C), long reaction times (sometimes 8–24 h), inert atmosphere or special chemicals such as a catalyst or toxic chemicals such as phenyl hydrazine [36]. Nevertheless, the synthesis sometimes involves complicated precursor, for example, synthesis of Ag(RCOO) from $AgNO_3$ and RCOOH [32]. All these reasons hamper the penetration of the technology in industrial production, particularly for the development of material systems employing a large numerical density of embedded contact-free nanoparticles. To overcome the aforementioned problems, precursors of metal silver, presenting fast thermolysis kinetics when dissolved in amorphous polystyrene, were searched for. The need for fast thermolysis kinetics is motivated by the fact that nanoparticles, by virtue of their large surface energy, tend to aggregate in low viscosity systems—the polystyrene matrix is fluid at the process temperature. The nanoparticle coalescence causes the splitting of the absorption peak into multiple SPR and light scattering phenomena if coagulation forms larger size nanoparticles [29]. The acetylacetonate (hereinafter acac) of silver was found to be an optimum precursor for this purpose—this study proves for the first time the complete thermal reaction of Ag-acac dissolved in concentrations as large as 1.2 wt% in molten PS to form contact-free silver nanoparticle in only 30 s at 200 °C. As a main result, in this communication, a nanocomposite material consisting of contact-free Ag-nanoparticles embedded in PS, characterized by a numerical particle density larger than 10^{+14}, resulting in an intense SPR absorption band is presented. In particular, the measured optical absorption exhibits a SPR resonance as narrow as 100 nm (FWHM) centred at 430 nm wavelength and an optimal transparency over the remnant part of the visible spectrum. The spectral photometric absorption curve shows unequivocally the presence of a very large density of contact-free Ag-nanoparticles which, to the best of our knowledge, has not previously been fabricated with either ex-situ or in situ methods. That the single narrow SPR absorption peak is directly linked to well separated, not coagulated, perfectly spherical silver nanoparticles has been corroborated here by microscopy analysis and quantitative topological analysis. Importantly, the negligible scattering indicates the presence of nanoparticles with diameter well below 50 nm. The optical properties of the material that has been developed, the simplicity (one-pot synthesis), cost-effectiveness, repeatability and scalability of the fabrication technology here developed, as well as its flexibility in being able to tailor the density of nanoparticles (from zero up to more than 10^{+14} nanoparticles per cm^3) make the in situ

thermolysis of Ag-acac in PS matrix a very promising technique for the development of high quality SPR optical limiters and filters.

In this study, commercial Ag-acac (Aldrich, 98% purity, $M_w = 206.98$), previously purified, was used to synthesize silver nanoparticles in molten PS. As the solubility of Ag-acac is modest in PS, to prepare the Ag-acac/PS blends, the silver precursor, available in crystalline powder form, was first dissolved in chloroform (Aldrich) and then the amorphous polystyrene (Aldrich, $M_w = 230{,}000$) was added in pellets to the solution. The resulting blends were then homogenized by constant stirring for 15 s in the case of diluted blends (0.08 wt% Ag-acac) and 60 s for the largest concentration experimented (1.2 wt% Ag-acac). The suspensions obtained in this way were then cast into petri dishes to form films of the same thickness (50 μm) and dried in air at 25 °C for several hours to let the solvent fully evaporate. Then, all the samples were thermally annealed on a hot-plate at a constant temperature of 200 °C. For all the concentrations investigated, the thermolysis of the precursor was always accompanied by a sudden colour change—light grey typical of Ag-acac/PS systems (see Fig. 1) to a transparent yellow typical of colloidal nanoscopic silver. Before annealing the samples, the thermolysis reaction of the precursor was studied in the presence of air and within the PS matrix to identify the optimal process temperature and duration. To this end, thermogravimetric analysis (TGA, TA instruments Q500) and dynamic-scanning calorimetry (DSC, TA instruments 2920) were performed by varying temperature at a rate of 0.16 °C/s. The Fig. 2a reports a DSC curve which shows that the thermolysis reaction of Ag-acac, in the presence of air, occurs suddenly in a burst when the material reaches a temperature of 140 °C; at this temperature the precursor material exchanges the whole reaction heat in a few seconds with the environment. Nevertheless, over the 150–300 °C temperature range the sample did not swap heat with the environment but, at the same time, it lost weight—apparent from the TGA measurement—the volatile by-products needed a few minutes to evaporate. The Fig. 2b reports the reaction heat exchanged during the thermolysis of Ag-acac dissolved in PS (1.2 wt%). The chemical reaction takes place approximately at the same temperature, but heat is released slower by the sample—considering that the PS releases heat slower than air, with a certain confidence, that the thermolysis of 1.2 wt% of Ag-acac in PS lasts less than 5 min at 140 °C can be assumed. Therefore, in order to precipitate very small silver nanoparticles, a high nucleation rate is required and the thermal annealing of Ag-acac/PS blends has been carried out isothermally at 200 °C. The samples fabricated were first analyzed by X-ray diffraction to evaluate the completion of the thermolysis reaction. In addition, transmission electron microscopy (TEM) was carried out. The Fig. 3a is a low magnification bright-field TEM image of the nanocomposite developed from 1.2 wt% of Ag-acac showing the homogeneity of the spatial distribution of nanoparticles within the PS matrix.

All samples were characterized by X-ray diffraction (XRD) using Cu-Kα radiation in the 2θ range 5–70°. Data

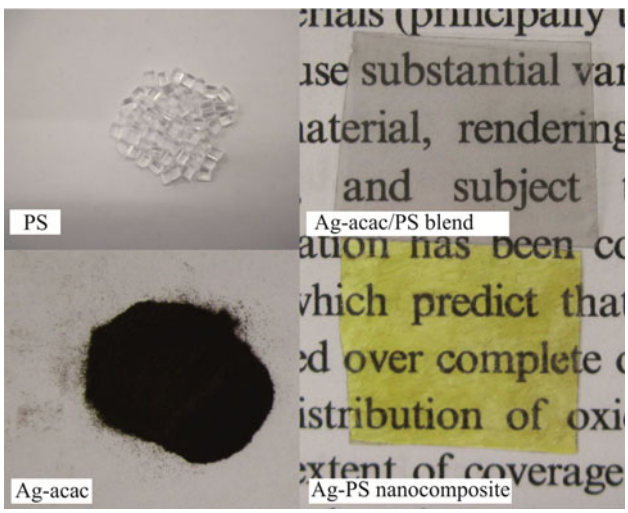

Fig. 1 Photography images of polystyrene (PS), silver-acetylacetonate (Ag-acac) precursor, Ag-acac/PS blend and Ag/PS nanocomposite synthesized from 1.2 wt% Ag-acac

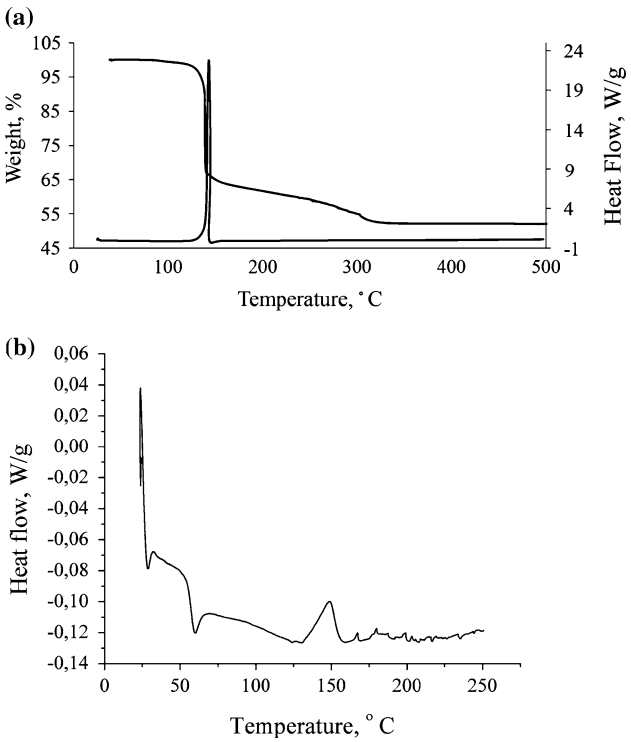

Fig. 2 DSC–TGA curves of pure Ag-acac sample in air (**a**) and DSC curve of the nanocomposite from 1.2 wt% Ag-acac (**b**)

were recorded with a PANalytical X'PertPRO diffractometer running in Bragg–Brentano geometry. Bright and dark field TEM (BF- and DF-TEM, respectively) imaging has been carried out to relate the optical behaviour of the nanocomposites to the spatial distribution of the embedded nanoparticles. Ultra-thin (70 ± 5 nm) film sections were microtomed at room temperature from the bulk nanocomposites using a Leica Ultracut UCT microtome. An FEI Tecnai T20 transmission electron microscope equipped with a LaB6 filament operating at 200 kV was used for BF imaging. An FEI Titan Analytical transmission electron microscope operating at 300 kV was used for DF imaging using a high angle annular dark field (HAADF) detector in scanning-transmission electron microscopy (STEM) mode. Microchemical analysis of the nanoparticles was carried out using energy dispersive X-ray spectroscopy (EDXS) in STEM mode. The Fig. 3b shows the XRD pattern of the Ag–PS nanocomposite developed from 1.2 wt% Ag-acac. The broad peak centred at $2\theta \sim 18$ is typical of polystyrene. The other narrow and intense peaks correspond to nanosilver diffraction pattern. No traces of non-reacted precursor are present. The XRD data are in accordance with the EDXS line scans performed on single nanoparticles (see Fig. 3c) with a spatial resolution of 5 Å as apparent from Fig. 3d. Specifically, the Fig. 3d shows the compositional variation (atom%) of Ag. As expected, a significant increase in the Ag signal is observed when carrying out line scans across the nanoparticles.

To detail at the nanoscale, and to quantify the size, shape and diameter distribution of the nanoparticles, as well as their spacing and homogeneity dispersion within the beam sensitive matrix, special microscopy techniques have been employed in this study. The TEM was operated in low-dose STEM mode: imaging was carried out using the HAADF technique to provide suitable high resolution images with atomic number contrast at short exposure times; spectroscopy was also achieved in STEM mode with acceptable X-ray count rates at very short line-scan times. These strategies of low-dose HAADF/STEM limited damage to the polymer nanocomposite during observation and analysis.

The Fig. 4a, b and d, e are two different magnifications of HAADF/STEM image of nanocomposites developed from 1.2 and 0.08 wt% of Ag-acac. The atomic number (Z) contrast results in bright spots corresponding to high Z silver nanoparticles in a dark low Z polymeric matrix. As shown in these micrographs, the nanoparticles are mostly well separated and contact free, whilst only a few might be aggregated—in fact, these few apparent aggregates (particles larger than 50 nm) may be due to image overlap of contact-free small particles located at different depths in

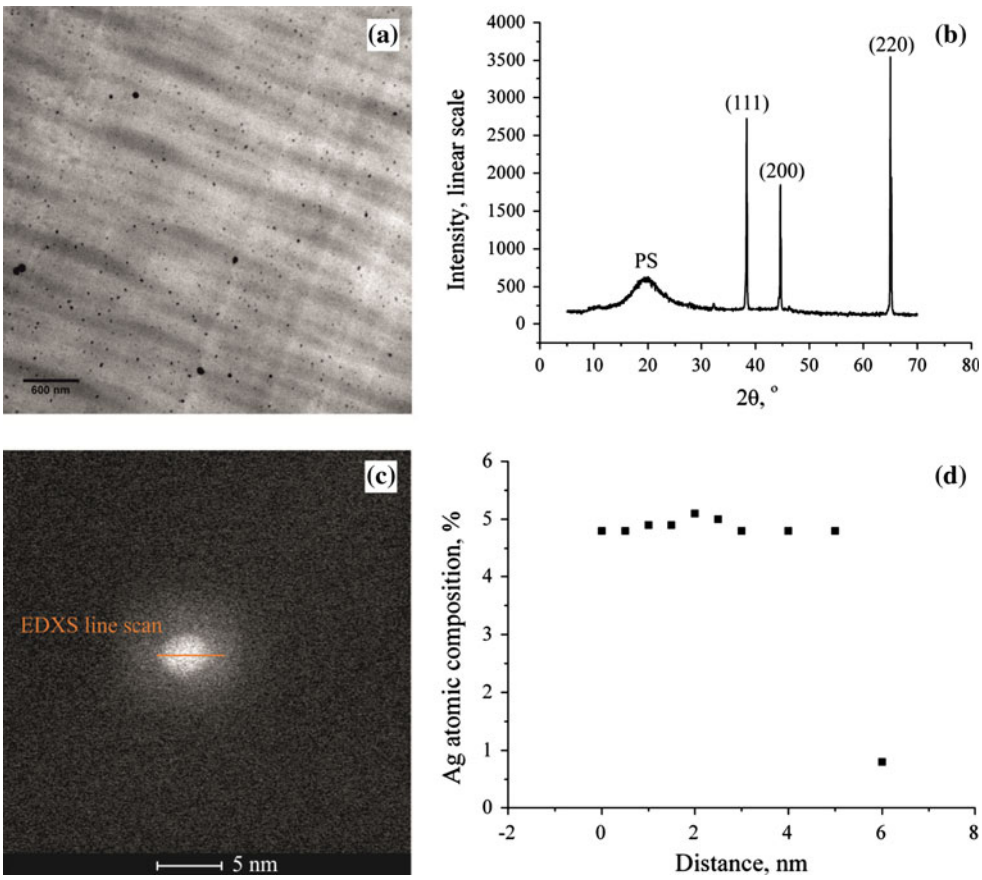

Fig. 3 Bright-field TEM image and XRD pattern of an Ag/PS nanocomposite (**a** and **b**, respectively). HAADF/STEM image of silver nanoparticles (**c**) and its atomic composition (%) (**d**) measured by EDXS along the line shown in **c**

the thin foil. To relate the microscopic analysis to the spectro-optical properties of the material fabricated, the nanoparticles were counted and classed according to their diameter. To this end, image analysis of over ten electron micrographs, covering a total specimen area of 35 μm squared (a volume of approx. 2500–3500 μm cubed assuming the foil thickness to be 70–100 nm), was performed by using the software OriginPro 8.1. The Fig. 4c, f plot the diameter distribution of Ag-nanoparticles generated in situ in a PS matrix from 1.2 and 0.08 wt% of precursor. The quantitative analysis shows that the nanoparticle diameters are similarly distributed independently on the precursor concentration which has generated them, however, a slight deviation of the relative peaks is acknowledged—the 0.08 wt% specimen has the most frequent diameter in the class ranging from 2 to 4 nm and the 1.2 wt% in the class from 1 to 2 nm. This difference can be explained on the basis of the LaMer theory [37]: for diluted blends the nucleation/growth processes dominate the saturation/supersaturation of the polymer matrix, and vice versa for the less diluted blends [38].

Table 1 reports that for both samples the minimum Ag diameter is 1.4 nm, whereas the maximum diameter corresponds to a few nanoparticle aggregates, or the microscopic projection of a large number of contact-free nanoparticles distributed along the specimen thickness. The particle size distribution is narrow and centred between 2 and 4 nm independently on precursor concentration, as shown in Fig. 4c, f.

The optical properties of the Ag–PS nanocomposite systems addressed in this study were characterized by spectrophotometry (UV–Vis Spectrophotometer Perkin-Elmer

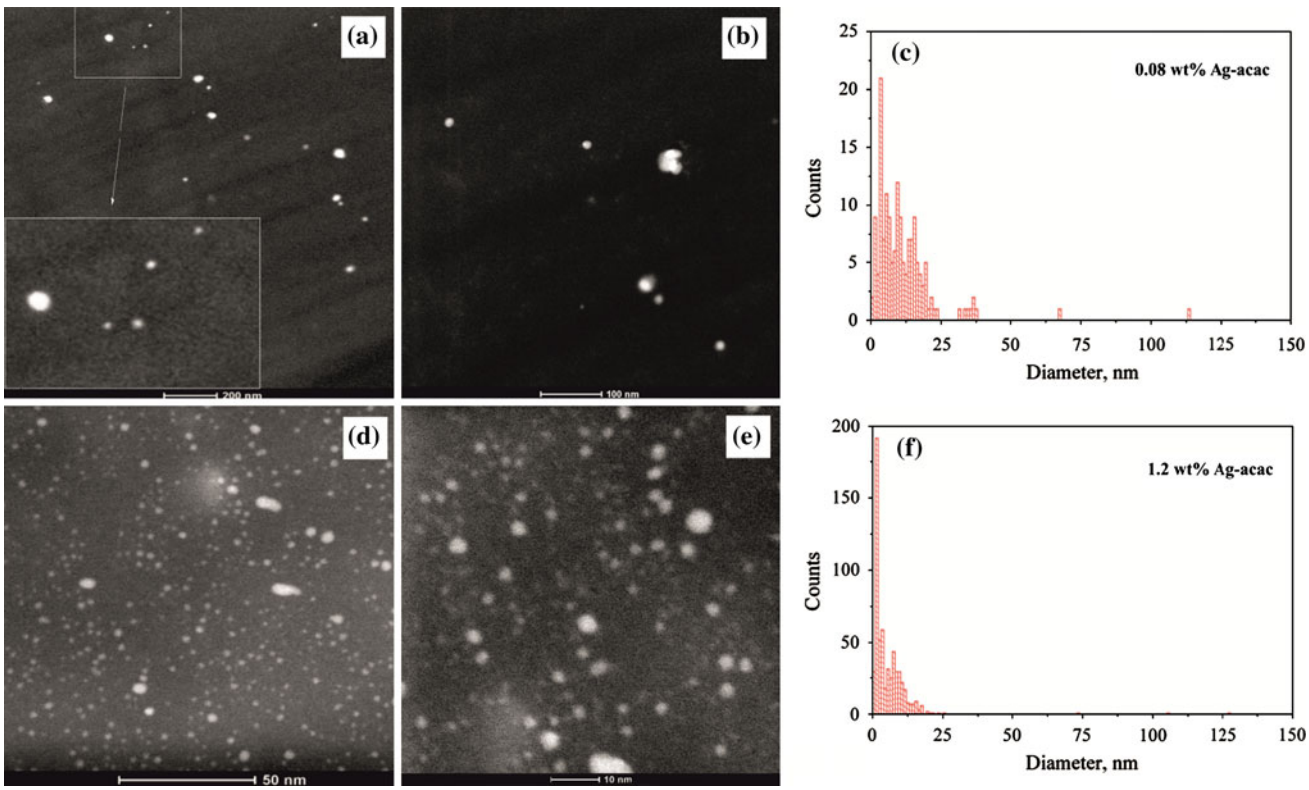

Fig. 4 HAADF/STEM micrographs of the Ag/PS nanocomposites from 0.08 wt% (**a**, **b**) and 1.2 wt% (**d**, **e**) Ag-acac. The metal nanoparticles are bright and the polymer matrix is dark. The particle size distributions of the Ag/PS nanocomposites from 0.08 and 1.2 wt% Ag-acac are shown in **c** and **f**, respectively

Table 1 Particle size analysis of the Ag-polystyrene nanocomposites fabricated from 0.08 and 1.2 wt% Ag-acac, Ag/PS-0.08 and Ag/PS-1.2, respectively

Sample Ag-acac	Wt%	No. Ag-NP for PSD	Min. dia. (nm)	Max. dia. (nm)	Stand. dev. (SD)
Ag/PS-0.08	0.08	159	1.4	195.3	18.9
Ag/PS-1.2	1.2	600	1.4	127.8	8.3

The table reports the number of particles, minimum and maximum diameter and standard deviation

Lambda 850). Figure 5 reports the spectral absorption of the Ag–PS nanocomposites synthesized from 0.08 and 1.2 wt% of Ag-acac. From this graph, it is apparent that the dependence of the materials' optical response on the shape and size of their nanofillers supports the behaviour deduced by Gustav Mie for the medium [39]. In fact in [40, 41], from the Mie's theory, it was found that for silver nanoparticles of diameter smaller than 40 nm that radiative processes are negligible, and particles only absorb energy at SPR; nevertheless, this material type starts scattering light when the size of the embedded nanoparticles is equal to 100 nm and larger. As for Fig. 5 and as corroborated by the quantitative topological analysis carried out in this study, only a few nanoparticles can diffuse the incident light—also the highest numerical density Ag–PS nanocomposites of this study exhibit extremely high transparency (the scattering is negligible). Always in accordance with the Mie's theory the light absorption is given by a single SPR, which is special case of spherical particles immersed in a dielectric associated with the homogenous displacement of the charges, yielding a dipolar charge distribution on the surface. These charges oscillate collectively giving rise to one proper resonance, which is determined uniquely by a spherical shape of the silver nanoparticles in situ synthesized, and their electron density.

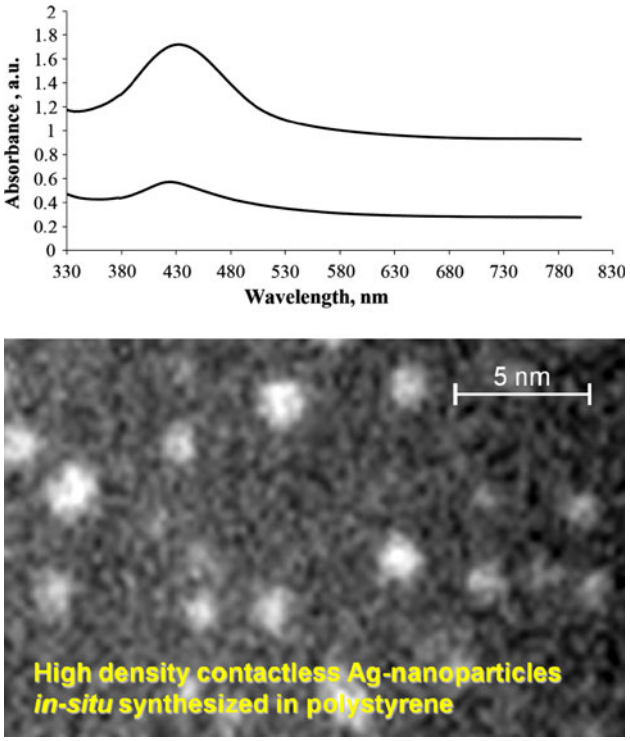

Fig. 5 Spectral absorbance of Ag/PS nanocomposites from 0.08 wt% (*lower curve*) and 1.2 wt% (*upper curve*)—data interval 1.00 nm; scan speed 266.75 nm/min

In fact, as the particle becomes less symmetric, the induced charge distribution on the surface can result not only on dipolar modes with different resonant frequencies, but also on higher multipolar charge distributions, even in the quasi-static limit [42]. The high multipolar SPR are always located at smaller wavelengths with respect to the dipolar one, which, in addition, is always red shifted by the presence of the electric field generated by the higher multipolar charge distributions. Recently, it has shown that a nanoparticle in a medium with refraction index $n > 1$ has SPR always red shifted with respect to those in vacuum [19]. Nevertheless, this shift depends on the proper mode itself: as the wavelength of the resonance increases, the red shift is greater, and the SPR are spread out. As the refractive index of optical polystyrene used in this study is 1.55 it should not astonish that the SPR of the materials developed here is located around 430 nm, red shifted by about 70, 75 nm from the peak of the same silver nanoparticles in vacuum [19]. A slight SPR red shift is also acknowledged for the sample of larger NP numerical density, fact which is probably linked to an increase of the effective refractive index due to the massive presence of particles in this material. As previously explained by Kreibig et al. [43–45] the SPR peak, extremely narrow for the nanocomposites fabricated here, is clear evidence of a very limited dispersion of the nanoparticle diameter and of the fact that the nanoparticles are contact free and not even coagulated as microscopy corroborates.

Conclusions

This study illustrates the fabrication of plasmonic Ag-nanocomposites by a high energy-transfer thermal degradation of Ag-acac in situ a PS matrix, a precursor of silver never reported so far for this purpose. This technology proved an outstanding flexibility at tailoring the numerical density of the embedded nanoparticles, and for all the precursor concentrations experimented; the process conditions found guarantee the synthesis of contact-free nanoparticles of size smaller than 40 nm, key element to obtain a single and narrow SPR, and a limited scattering over the whole visible spectrum. The technology developed, as being compatible with the surface micromachining technology can be straightforwardly harnessed for the development of custom, extremely thin, optical limiters or filters for the production of optical MEMS and NEMS.

Acknowledgements The authors thank the Center for Electron Nanoscopy of the Technical University of Denmark. The study reported in this communication is partly underpinned by the Directorate for Research of the European Commission in the frame of VII framework program under the contract: 213436-project acronym: Nanotough.

References

1. Baekeland LH (1909) Sci Am 68:322
2. Goodyear C (1856) Dinglers Polytech J 139:376
3. Usuki A, Kojima M, Okada A, Fukushima Y, Kamigaito O (1993) J Mater Res 8:1179
4. Kojima Y, Usuki A, Kawasumi M, Okada A, Fukushima Y, Kurauchi T, Kamigaito O (1993) J Mater Res 8:1185
5. Martorana B, Carotenuto G, Pullini D, Zvezdin K, La Peruta G, Perlo P, Nicolais L (2006) Sens Actuators A Phys 129:176
6. Martorana B, Carotenuto G, Pullini D, Zvezdin K, La Peruta G, Perlo P, Nicolais L (2005) Polym News 30:394
7. Shi S, Ji W, Tang SH, Lang JP, Xin XQ (1994) J Am Chem Soc 116:3615
8. Yu DB, Sun XQ, Bian JT, Tong ZC, Qian YT (2004) Phys E Low Dimens Syst Nanostruct 23:50
9. Koch SW, Peyghambarian N, Gibbs HM (1988) J Appl Phys 63:R1
10. Prasad PN (2004) Nanophotonics. Wiley, Hoboken, NJ
11. Tutt LW, Boggess TF (1993) Prog Quantum Electron 17:299
12. Sun YP, Riggs JE, Rollins HW, Guduru R (1999) J Phys Chem B 103:77
13. Grady NK, Halas NJ, Nordlander P (2004) Chem Phys Lett 399:167
14. Brongersma ML, Hartman JW, Atwater HA (2000) Phys Rev B 62:R16356
15. Carotenuto G, Nicolais L (2004) Compos B Eng 35:385
16. de Leon AG, Dirix Y, Staedler Y, Feldman K, Hahner G, Caseri WR, Smith P (2000) Appl Opt 39:4847
17. Dirix Y, Darribere C, Heffels W, Bastiaansen C, Caseri W, Smith P (1999) Appl Opt 38:6581
18. Zimmermann L, Weibel M, Caseri W, Suter UW (1993) J Mater Res 8:1742
19. Gonzales AL, Noguez C (2007) Phys Stat Sol (c) 4:4118
20. Smitha SL, Nissamudeen KM, Philip D, Gopchandran KG (2008) Spectrochim Acta A 71:186
21. Zhao Y, Jiang Y, Fang Y (2006) Spectrochim Acta A 65:1003
22. Evanoff DD, Chumanov G (2005) Chemphyschem 6:1221
23. Carotenuto G, Nicolais L (2006) Metal–polymer nanocomposites. John Wiley & Sons, Inc., Hoboken, NJ
24. Shim IK, Lee YI, Lee KJ, Joung J (2008) Mater Chem Phys 110:316
25. Yamamoto M, Nakamoto M (2003) J Mater Chem 13:2064
26. Hiramatsu H, Osterlok FE (2004) Chem Mater 16:2509
27. Lee KJ, Jun BH, Choi J, Lee YI, Joung J, Oh YS (2007) Nanotechnology 18:335601/1
28. Lee SJ, Han SW, Kim K (2002) Chem Commun 5:442
29. Navaladian S, Viswanathan B, Viswanath RP, Varadarajan TK (2007) Nanoscale Res Lett 2:44
30. D'Urso L, Nicolosi V, Compagnini G, Puglisi O (2004) Appl Surf Sci 226(c):131
31. Chen Z, Gao L (2007) Mater Res Bull 42:1657
32. Yamamoto M, Kashiwagi Y, Nakamoto M (2006) Langmuir 22:8581
33. Chen M, Feng YG, Wang X, Li TC, Zhang JY, Qian DJ (2007) Langmuir 23:5296
34. Kashiwagi Y, Yamamoto M, Nakamoto M (2006) J Colloid Interface Sci 300:169
35. Yang N, Aoki K (2005) J Phys Chem 109:23911 B
36. Li Y, Wu Y, Ong BS (2005) J Am Chem Soc 127:3266
37. La Mer VK (1952) Ind Eng Chem 6:1270
38. Fievet F, Lagier JP, Figlarz M (2009) Mater Res Soc Bull 14:29
39. Mie G (1908) Ann Phys (Leipz) 25:377
40. Gonzalez AL, Noguez C (2007) Phys Stat Sol C 11:4
41. Noguez C (2005) Opt Mater 27:1204
42. Fuchs R (1975) Phys Rev B 11:1732
43. Schonauer D, Quinten M, Kreibig U (1989) Z PhysAtoms Mol Clust 12:527
44. Chaudhary V, Thakur AK, Bhowmick AK (2011) J Mater Sci 46:6096. doi:10.1007/s10853-011-5573-x
45. Mondal B, Saha SK (2011) J Mater Sci 46:5153. doi:10.1007/s10853-011-5446-3